

Performance Evaluation and Optimization of LPWA IoT Networks: A Stochastic Geometry Approach

Amin Azari and Cicek Cavdar

KTH Royal Institute of Technology, Email: {aazari, cavdar}@kth.se

Abstract—Leveraging grant-free radio access for enabling low-power wide-area (LPWA) Internet of Things (IoT) connectivity has attracted lots of attention in recent years. Regarding lack of research on LPWA IoT networks, this work is devoted to reliability modeling, battery-lifetime analysis, and operation-control of such networks. We derive the interplay amongst density of the access points, communication bandwidth, volume of traffic from heterogeneous sources, and quality of service (QoS) in communications. The presented analytical framework comprises modeling of interference from heterogeneous sources with correlated deployment locations and time-frequency asynchronous radio-resource usage patterns. The derived expressions represent the operation regions and rates in which, energy and cost resources of devices and the access network, respectively, could be traded to achieve a given level of QoS in communications. For example, our expressions indicate the expected increase in QoS by increasing number of transmitted replicas, transmit power, density of the access points, and communication bandwidth. Our results further shed light on scalability of such networks and figure out the bounds up to which, scaling resources can compensate the increase in traffic volume and QoS demand. Finally, we present an energy-optimized operation control policy for IoT devices. The simulation results confirm tightness of the derived analytical expressions, and indicate usefulness of them in planning and operation control of IoT networks.

Index Terms—5G, Coexistence, Grant-free, Reliability and durability, LPWA IoT.

I. INTRODUCTION

Providing connectivity for massive Internet-of-Things (IoT) devices is a key driver of 5G [1]. Until now, several solutions have been proposed for enabling large-scale IoT connectivity, including evolutionary and revolutionary solutions [2]. Evolutionary solutions aim at enhancing connectivity procedure of existing LTE networks, e.g. access reservation and scheduling improvement [3, 4]. On the other hand, revolutionary solutions aim at providing scalable low-power IoT connectivity by redesigning the access network. In 3GPP LTE Rel. 13, narrowband IoT (NB-IoT) has been announced as a revolutionary solution which handles communications over a 200 KHz bandwidth [5]. This narrow bandwidth brings high link budget, and offers extended coverage [5]. To provide autonomous low-latency access to radio resources, grant-free radio access is a study item in 3GPP IoT working groups, and it is expected to be included in future 3GPP standards [6]. Thanks to the simplified connectivity procedure, and removing the need for pairing and fine synchronization, grant-free radio access has attracted lots of interests in recent years for providing low-power ultra-durable IoT connectivity, especially when more than 10 years lifetime is required. SigFox and LoRa are two

dominant grant-free radio access solutions over the public ISM-band, which is used for industrial, scientific, and medical purposes [2]. While energy consumptions of LoRa and SigFox solutions are extremely low, and their provided link budget is enough to penetrate to most indoor areas, e.g. LoRa signal can be decoded when it is 20 dB less than the noise level, reliability of their communications in coexistence scenarios is questionable [7, 8]. [7] presents experimental measurements in such coexistence scenarios, where multiple IoT technologies are sharing a set of radio resources, and confirms significant impact of interference on IoT communications. Regarding the growing interest in grant-free radio access for IoT communications in public and proprietary cellular networks [2, 6], it is required to investigate the reliability, battery lifetime, and scalability of such networks in serving multi-type IoT devices.

A. Literature Study

Non-orthogonal radio access has attracted lots of attentions in recent years as a complementary radio access scheme for future generations of wireless networks [9, 10]. In literature, non-orthogonal access has been mainly employed in order to increase the network throughput [11], reliability [12], battery lifetime [13], and reduce access delay [11] in serving non-IoT traffic. In [14], grant-free access to uplink radio resources of cellular networks has been analyzed for intra-group communications of IoT devices. In [13], a novel receiver for grant-free radio access IoT networks has been designed, which benefits from oscillator imperfection of cheap IoT devices for contention resolution. In [15], outage probability in grant-free access has been studied by assuming a constant received power from all contending devices, which is not the case in practice regarding the limited transmit-power of IoT devices, as well as lack of channel state information at the device-side for power control. The success probability in grant-free radio access has been also analyzed in [8, 16] by assuming a Poisson point process (PPP) distribution of IoT devices.

One sees the research on grant-free radio access has been mainly focused on success probability analysis in homogeneous scenarios, and there is lack of research on performance analysis of large-scale IoT networks with multi-type IoT devices with heterogeneous communications characteristics. Furthermore, when it comes to the distribution of devices in wide-area IoT networks, PPP has been mainly used. However, this assumption may lead to inaccurate results [17, 18] due to the cell ranges that can go up to tens of kilometers [2] and hot-spots. In hot-spots, e.g. buildings and shopping centers, a high

density of IoT devices exist; while outside them, a low density of devices exists. Then, a Poisson cluster process (PCP), which takes the correlation between locations of devices into account, suits well for the distribution process of devices in LPWA IoT networks [17, 18].

B. Contributions

Here, we address an important problem, not tackled previously: network design in coexistence scenarios with grant-free radio access. Enabling IoT connectivity requires deployment of access points (APs) and allocation of frequency resources, which increase the network costs. On the other hand, the experienced delay, consumed energy, and success of IoT applications have strong couplings with reliability of data transfer, which is a function of provisioned network resources. This tradeoff is investigated in this work. The main contributions of this work include:

- Provide a rigorous analytical model of reliability for heterogeneous LPWA IoT networks in terms of provisioned resources, e.g. density of the APs, and characteristics of traffic, e.g. activity factor of each traffic type.
- Provide an analytical model of battery lifetime for IoT devices in terms of device's parameters, e.g. battery capacity, and network parameters, e.g. reliability of communications.
- Analyze the tradeoffs among network cost, battery lifetime, and reliability of communications. Present the operation regions in which tuning a communication parameter, e.g. number of replica transmissions, increases both reliability and battery lifetime, offers a tradeoff between them, and decreases both of them.
- Propose a reliability-constrained lifetime-optimized operation control policy for IoT devices.
- Analyze scalability of the network. Figuring out the bounds up to which, scaling network's and devices' resources can compensate the increase in traffic volume and QoS demand.

The remainder of paper has been organized as follows. System model and problem description are presented in the next section. Modeling of KPIs is presented in section III. Section IV presents the optimized operation control strategies. Simulation results are presented in section V. Concluding remarks are given in section VI.

II. SYSTEM MODEL AND PROBLEM DESCRIPTION

A. System Model

A set of IoT devices, denoted by Φ , have been distributed according to different spatial PCPs in a wide service area. Φ comprises of K subsets, Φ_k for $k \in \mathcal{K} \triangleq \{1, \dots, K\}$, where each subset refers to a specific type of IoT service. Traffic from different subsets differ in the way they use the time-frequency resources, i.e. in frequency of packet generation $1/T_k$, signal bandwidth w_k , packet transmission time τ_k ,

number of replicas¹ transmitted per packet n_k , and transmit power P_k . Subscript k refers to the type of IoT devices. For PCP of type- k IoT traffic, the $(\lambda_k, v_k, f(\mathbf{x}))$ tuple characterizes the distribution process in which, λ_k is the density of the parent points and v_k is the average number of daughter points per parent point², as defined in [18]. Also, $f(\mathbf{x})$ is an isotropic function representing scattering density of the daughter points around a parent point, e.g. a normal distribution:

$$f(\mathbf{x}) = \exp(-\|\mathbf{x} - \mathbf{x}_0\|^2 / (2\sigma^2)) / \sqrt{2\pi\sigma^2}, \quad (1)$$

where σ is the variance of distribution and \mathbf{x}_0 is the location of parent point. A frequency spectrum of W is shared for communications, on which the power spectral density of noise is denoted by \mathcal{N} . We aim at collecting data from a subset of \mathcal{K} , denoted by ϕ , where $|\phi| \leq |\mathcal{K}|$. Devices in ϕ may also share a set of semi-orthogonal codes denoted by ϖ with cardinality $|\varpi|$, which reduces the interference from other devices reusing the same radio resource with a different code by factor of Q . Examples of such codes are semi-orthogonal spreading codes in LoRa technology [2].

III. ANALYTICAL MODELING OF KPIs

A. Modeling of Reliability

In the grant-free radio access system, transmitting devices are asynchronous in time and frequency domains, and hence, the received packets at the receiver could have partial overlaps in time-frequency. To model reliability in communications, we first derive analytical models for interference in subsection III-A1, and for probability of success in subsection III-A2. These models are then employed in deriving reliability of communications in subsection III-A3.

1) *Interference Analysis*: We assume a type- i device has been located at point \mathbf{z} in a 2D plane, and its respective AP has been located at the origin. In order to derive probability of success in data transmission from the device to the AP, we need to characterize the received interfere at the AP. A common practice in interference analysis is to determine its moments, which is possible by finding its generating function, i.e. the Laplace functional [17, 19]. Towards this end, let us introduce three stationary and isotropic processes: i) $\Psi^{(1)} = \cup_{k \in \mathcal{K}} \Psi_k^{(1)}$, where $\Psi_k^{(1)}$ represents the PCP containing locations of type- k transmitting nodes which are reusing radio resources with a similar code to the code³ of transmitter of interest; ii) $\Psi^{(2)} = \cup_{k \in \mathcal{K}} \Psi_k^{(2)}$, where $\Psi_k^{(2)}$ represents the PCP containing locations of type- k transmitting nodes which are reusing radio resources with a different code (or no code,

¹Practical motivations for modeling such replicas can be found in state of the art IoT technologies like NB-IoT and SigFox in which, coverage extension and resilience to interference are achieved by repetitions of transmitted packets [2, 5]. When it is not the case, $n_k = 1$ can be used.

²In PCP deployment, we have clusters of devices, where each cluster models a hot-spot. λ_k represents density of such clusters of devices, i.e. the parent points. v_k represents the average number of devices in each cluster, i.e. the daughter points. Finally, $f(x)$ represents how devices are distributed in each cluster.

³Note: as mentioned in the system model, devices in ϕ share a set of semi-orthogonal codes for partial interference management.

in case $k \notin \phi$) than the transmitter of interest; and iii) $\Psi = \cup_{j \in \{1,2\}} \Psi_k^{(j)}$. For an AP located at the origin, the Laplace functional of the received interference at the receiver is given by:

$$\mathcal{L}_{I_\Psi}(s) = \mathbb{E}[\exp(-sI_\Psi)] \quad (2)$$

$$= \mathbb{E}[\prod_{j \in \{1,2\}} \prod_{k \in \mathcal{K}} \prod_{\mathbf{x} \in \Psi_k^{(j)}} \mathcal{L}_h(sQ_j P_k g(\mathbf{x}))],$$

where $Q_j P_k g(\mathbf{x})$ is the average received power due to a type- k transmitter at point \mathbf{x} , $Q_1 = 1$, $Q_2 = Q$, and Q is the rate of rejection of interference between two devices with different multiple access codes, as defined in section II-A. Also, h is the power fading coefficient associated with the channel between the device and the AP, and $\mathcal{L}_h(sQ_j P_k g(\mathbf{x}))$ is the Laplace functional of the received power. We consider the following general path-loss model $g(\mathbf{x}) = 1/(\alpha_1 + \alpha_2 \|\mathbf{x}\|^\delta)$, where δ is the pathloss exponent, and α_1 and α_2 are control parameters. When h follows Nakagami- m fading, with the shaping and spread parameters of $m \in \mathbb{Z}^+$ and $\Omega > 0$ respectively, the probability density function (PDF) of the power fading coefficient is given by:

$$p_h(q) = \frac{1}{\Gamma(m)} \left(\frac{m}{\Omega}\right)^m q^{m-1} \exp\left(-\frac{mq}{\Omega}\right), \quad (3)$$

where Γ is the Gamma function. Then, using Laplace table, $\mathcal{L}_h(sQ_j P_k g(\mathbf{x}))$ is derived as:

$$L_h(sQ_j P_k g(\mathbf{x})) = (1 + \Omega s P_k g(\mathbf{x})/m)^{-m}. \quad (4)$$

By inserting (4) in (2) and considering the fact that the received interferences from different devices are independent, we have:

$$\mathcal{L}_{I_\Psi}(s) = \prod_{j,k} \mathbb{E}_{\mathbf{x},\mathbf{y}} \left[\prod_{\mathbf{y} \in \Theta_k} \left(\prod_{\mathbf{x} \in \theta_{\mathbf{y}}^{(j)}} u(\mathbf{x}, \mathbf{y}) \right) \right],$$

where $k \in \mathcal{K}$, $j \in \{1,2\}$, the set of parent points of type- k is denoted by Θ_k , and transmitting nodes which are daughter points of y as $\theta_{\mathbf{y}}^{(j)}$. Also, \mathbb{E}_x represents expectation over x , and

$$u(\mathbf{x}, \mathbf{y}) = (1 + \Omega s Q_j P_k g(\mathbf{x} - \mathbf{y})/m)^{-m}.$$

The received interference over the packet of interest can be decomposed into two parts: i) interference from transmitters belonging to the cluster of transmitter, i.e. daughter points of the same parent point; and ii) other transmitters. Let us denote the Laplace functional of interference from the former and latter transmitters as $\mathcal{L}_{I_\Psi}^\dagger(s)$ and $\mathcal{L}_{I_\Psi}^\ddagger(s)$ respectively. Then, we have:

$$\mathcal{L}_{I_\Psi}(s) = \mathcal{L}_{I_\Psi}^\ddagger(s) \mathcal{L}_{I_\Psi}^\dagger(s). \quad (5)$$

Using equation (18) in [17], and by conditioning on Θ_k and $\theta_{\mathbf{y}}^{(j)}$, one has:

$$\mathcal{L}_{I_\Psi}^\dagger(s) \quad (6)$$

$$= \prod_{j,k} \mathbb{E}_y \left[\prod_{\mathbf{y} \in \Theta_k} \left\{ \exp\left(-\hat{v}_{k,j} \int_{\mathbb{R}^2} [1-u(\mathbf{x}, \mathbf{y})] f(\mathbf{x}) d\mathbf{x}\right) \right\} \right],$$

$$= \exp\left(-\sum_{j,k} \lambda_k \int_{\mathbb{R}^2} \left\{ 1 - \exp\left(-\hat{v}_{k,j} \int_{\mathbb{R}^2} [1-u(\mathbf{x}, \mathbf{y})] f(\mathbf{x}) d\mathbf{x}\right) \right\} d\mathbf{y}\right).$$

Also, in (6) the average numbers of interfering type- k devices in each cluster for $j \in \{1,2\}$ are denoted as $\hat{v}_{k,1} = v_k \frac{n_k \tau_k}{T_k} \frac{w_k}{W} \frac{1}{|\varpi|}$ and $\hat{v}_{k,2} = v_k \frac{n_k \tau_k}{T_k} \frac{w_k}{W} \frac{|\varpi|-1}{|\varpi|}$ for $k \in \phi$. In these two expressions, the first fraction represents the percentage of time in which device is active, i.e. the time activity factor, the second fraction represents the ratio of bandwidth that device occupies in each transmission, i.e. the frequency activity-factor, and the third fraction represents the code-domain activity factor, i.e. the probability that two devices select the same code, i.e. $\frac{1}{|\varpi|}$, or different codes $\frac{|\varpi|-1}{|\varpi|}$. Then, for $k \notin \phi$, in which devices don't share semi-orthogonal codes for communications, it is clear that $\hat{v}_{k,1} = 0$, and $\hat{v}_{k,2} = v_k \frac{n_k \tau_k}{T_k} \frac{w_k}{W}$. Following the same procedure used for deriving $\mathcal{L}_{I_\Psi}^\ddagger(s)$, one can derive $\mathcal{L}_{I_\Psi}^\dagger(s)$ as:

$$\mathcal{L}_{I_\Psi}^\dagger(s) = \prod_{j \in \{1,2\}} \mathbb{E}_y \left[\mathbb{E}_x \left[\prod_{\mathbf{x} \in \theta_{\mathbf{y}}^{(j)}} u(\mathbf{x}, \mathbf{y}) \right] \right] \quad (7)$$

$$= \int_{\mathbb{R}^2} \exp\left(-\sum_j \hat{v}_{i,j} \int_{\mathbb{R}^2} (1-u(\mathbf{x}, \mathbf{y})) f(\mathbf{x}) d\mathbf{x}\right) f(\mathbf{y}) d\mathbf{y}.$$

2) *Probability of Success in Transmission:* Let N denote the additive noise at the receiver. Using the interference model, probability of success in packet transmission of a type- i device, located at \mathbf{z} , to the AP, located at the origin, is:

$$p_s(i, \mathbf{z}) = \Pr(P_i h g(\mathbf{z}) \geq [N + I_\Psi] \gamma_{\text{th}}) \quad (8)$$

$$\stackrel{(a)}{=} \sum_{\nu=0}^{m-1} \frac{1}{\nu!} \int_0^\infty \exp\left(-\frac{\gamma_{\text{th}} m q}{\Omega P_i g(\mathbf{z})}\right) q^\nu d\Pr(I_\Psi + N \geq q)$$

$$\stackrel{(b)}{=} \sum_{\nu=0}^{m-1} \frac{(-1)^\nu}{\nu!} [\mathcal{L}_{I_\Psi}(s) \mathcal{L}_N(s)]^{(\nu)} \Big|_{s=\frac{\gamma_{\text{th}} m}{\Omega P_i g(\mathbf{z})}},$$

where $[F(s)]^{(\nu)} = \frac{\partial^\nu}{\partial s^\nu} F(s)$, (a) follows from [19, Appendix C] and equation (3) in which $p_h(q)$ has been defined, and finally (b) follows from [20, Lemma 3.1] and the fact that $\mathcal{L}(t^n f(t)) = (-1)^n \frac{\partial^n}{\partial s^n} F(s)$. Furthermore, L_{I_Ψ} has been characterized in (6) and (7), and $\mathcal{L}_N(s)$ is the Laplace transform of noise. In order to get insights on how coexisting services affect each other, in the following we focus on $m = 1$, i.e. the Rayleigh fading, and present a closed-form approximation of the success probability. In section V, we will evaluate tightness of this expression.

Theorem 3.1: For $m = 1$, success probability in packet transmission can be approximated as:

$$p_s(i, \mathbf{z}) \approx P_N \left[\exp\left(-\sum_{j \in \{1,2\}} \sum_{k \in \mathcal{K}} \lambda_k \hat{v}_{k,j} H(\mathbf{z}, 1, \frac{Q_j P_k \gamma_{\text{th}}}{\Omega P_i})\right) \right]$$

$$\times \exp\left(-\sum_{j \in \{1,2\}} \hat{v}_{i,j} H(\mathbf{z}, f^*(\mathbf{x}), \frac{Q_j \gamma_{\text{th}}}{\Omega})\right), \quad (9)$$

where $f^*(\cdot) = \text{conv}(f(\cdot), f(\cdot))$,

$$H(\mathbf{z}, f^*(\mathbf{x}), \xi) = \int_{\mathbf{x} \in \mathbb{R}^2} \frac{g(\mathbf{x})}{g(\mathbf{x}) + g(\mathbf{z})/\xi} f^*(\mathbf{x}) d\mathbf{x}, \quad (10)$$

$$P_N = \exp\left(-\mathcal{N}_{\gamma_{\text{th}}/[\Omega P_i g(\mathbf{z})]}\right), \quad (11)$$

and \mathcal{N} is the noise power.

Proof The proof is given in theorem 3.2 of the extended version [21].

$H(\mathbf{z}, f^*(\mathbf{x}), \xi)$ and $H(\mathbf{z}, 1, \xi)$ could be derived in closed-form for most well-known pathloss and distribution functions, as follows.

Corollary 3.2: For $g(\mathbf{x}) = \alpha \|\mathbf{x}\|^{-\delta}$,

$$H(\mathbf{z}, 1, \xi) = \|\mathbf{z}\|^2 \xi^{\frac{2}{\delta}} 2\pi^2 \csc(2\pi/\delta) / \delta. \quad (12)$$

Proof By change of coordinates, $\mathbf{x} \rightarrow (r, \theta)$, we have:

$$\begin{aligned} H(\mathbf{z}, 1, \xi) &= \int_{\mathbf{x} \in \mathbb{R}^2} \frac{\alpha \|\mathbf{x}\|^{-\delta}}{\alpha \|\mathbf{x}\|^{-\delta} + \alpha \|\mathbf{z}\|^{-\delta} / \xi} d\mathbf{x}, \\ &= 2\pi \int_0^\infty \frac{1}{1 + (r/\|\mathbf{z}\|)^\delta / \xi} r dr. \end{aligned}$$

Solving this integral by using [22, Eq. 3.352], (12) is derived. ■

Corollary 3.3: For $g(\mathbf{x}) = \alpha \|\mathbf{x}\|^{-4}$, and $f(\mathbf{x})$ given in (1),

$$\begin{aligned} H(\mathbf{z}, f^*(\mathbf{x}), \xi) &= \frac{\|\mathbf{z}\|^2}{4\sigma^2 \sqrt{\xi}} \left[\text{ci}\left(\frac{\|\mathbf{z}\|^2}{4\sigma^2 \sqrt{\xi}}\right) \sin\left(\frac{\|\mathbf{z}\|^2}{4\sigma^2 \sqrt{\xi}}\right) - \right. \\ &\quad \left. \text{si}\left(\frac{\|\mathbf{z}\|^2}{4\sigma^2 \sqrt{\xi}}\right) \cos\left(\frac{\|\mathbf{z}\|^2}{4\sigma^2 \sqrt{\xi}}\right) \right], \end{aligned}$$

where $\text{si}(\cdot)$ and $\text{ci}(\cdot)$ are well-known sine and cosine integrals, as follows:

$$\text{si}(x) = - \int_x^\infty \frac{\sin(t)}{t} dt, \quad \text{ci}(x) = - \int_x^\infty \frac{\cos(t)}{t} dt.$$

Proof The proof is given in corollary 3.4 of the extended version [21].

Remark Analysis of $H(\mathbf{z}, f^*(\mathbf{x}), \xi)$ shows that it can be well approximated by 1 for $\frac{\sqrt{\xi} \|\mathbf{z}\|^2}{4\sigma^2} \gg 1$. For theorem 3.1 in which $\xi = Q_j \gamma_{\text{th}} / \Omega$, $H(\mathbf{z}, f^*(\mathbf{x}), \xi) \approx 0$ for $j = 1$ because $Q_1 = Q \approx 0$; and $H(\mathbf{z}, f^*(\mathbf{x}), \xi) \approx 1$ for $j = 2$ when $z \gg z_0 \triangleq \frac{2\sigma \sqrt[4]{\Omega}}{\sqrt[4]{\gamma_{\text{th}}}}$ because $Q_2 = 1$.

Remark From theorem 3.1, one sees that probability of success, $p_s(i, \mathbf{z})$, is a function of $\|\mathbf{z}\|$ rather than phase of \mathbf{z} . Then, hereafter we use $p(i, z)$ to denote probability of success for communication distance of z .

Until now, we have derived the probability of success for a given communication distance to an AP. In the following, we investigate success probability where multiple APs might be able to decode a packet, i.e. the coverage areas of neighboring APs are overlapping. Regarding the fact that theorem 3.1 provides probability of success as a function of communication distance, given the distribution process of APs, the expected communication distance to the neighboring APs, and hence, probability of success in data transmission could be derived. In PPP deployment of APs with density λ_a , the PDF of distance from a random point to the ℓ th nearest AP, denoted by d_ℓ is given by [23]:

$$P_{d_\ell}(r) = \exp(-\lambda_a \pi r^2) 2(\lambda_a \pi r^2)^\ell / [r(\ell - 1)!].$$

Then, one can derive the average probability of success in packet transmission from a random point for type- i as:

$$P_s(i) = 1 - \prod_{\ell=1}^{\ell_{\max}} \int_0^\infty (1 - p_s(i, r)) P_{d_\ell}(r) dr. \quad (13)$$

Theorem 3.4: For $f(x)$ given in (1), and $g(\mathbf{z}) = \alpha \|\mathbf{z}\|^{-4}$, we have:

$$P_s(i) \approx 1 - \prod_{\ell=1}^{\ell_{\max}} \left[1 - \frac{X_0}{\sqrt{X_1}^{\ell-1}} \exp\left(\frac{X_2^2}{4X_1^2}\right) \mathcal{G}(X_3, \ell) \right],$$

where $X_0 = \frac{(\lambda_a \pi)^\ell}{(\ell - 1)!} \exp(-\hat{v}_{i,2})$, $X_1 = \frac{\mathcal{N} \gamma_{\text{th}}}{\Omega P_i \alpha}$,

$$X_2 = \sum_{j,k} \lambda_k \hat{v}_{k,j} \left(\frac{\gamma_{\text{th}} Q_j P_k}{\Omega P_i} \right)^{0.5} \frac{\pi^2}{2} \csc\left(\frac{\pi}{2}\right) + \lambda_a \pi, \quad X_3 = \frac{X_2}{2\sqrt{X_1}}.$$

Also, $\mathcal{G}(X_3, \ell) = \int_{\frac{X_2^2}{2X_1}}^\infty (z - X_3)^{(\ell-1)} \exp(-z^2) dz$, and could be derived for any ℓ in the form of error function, e.g. for $\ell_{\max} = 2$:

$$\mathcal{G}(X_3, 1) = -(\sqrt{\pi}(\text{erf}(X_3) - 1))/2,$$

$$\mathcal{G}(X_3, 2) = \exp(-X_3^2)/2 + (X_3 \sqrt{\pi}(\text{erf}(X_3) - 1))/2.$$

Proof The proof is given in theorem 3.5 of the extended version [21].

3) *Reliability of IoT Communication:* Now, we have the required tools to investigate reliability of IoT communications. Once a type- i device has a packet to transmit, it transmits n_k replicas of the packet, and listens for ACK from the AP(s). If No ACK is received in a bounded listening window, device retransmits the packet, and this procedure could be repeated up to $B_i - 1$ times, where the bound may come from the fair use of the shared medium [2, 7] or expiration of data. If data transmission is unsuccessful in B_i attempts, we call it an outage event. The probability of outage for type i in such setting could be derived as:

$$P_o(i) = [1 - P_s(i)]^{n_i B_i}, \quad (14)$$

where $P_s(i)$ has been derived in theorem 3.4.

B. Battery Lifetime Performance (Durability)

Packet generation at each device for most reporting IoT applications can be seen as a Poisson process [24]. Then, one can model energy consumption of a device as a semi-regenerative process where the regeneration point has been located at the end of each successful data transmission epoch [4]. For a given device of type- i , let us denote the stored energy in batteries as E_0 , static energy consumption per reporting period for data acquisition from environment and processing as E_{st} , circuit power consumption in transmission mode as P_c , and inverse of power amplifier efficiency as η . Then, the expected battery lifetime is [4]:

$$\mathbb{L}(i) = \frac{E_0}{E_{\text{st}} + \hat{\beta}_i E_c + \hat{\beta}_i n_i (\eta P_i + P_c) \tau_i} T_i, \quad (15)$$

where E_c represents the average energy consumption in listening after each trial for ACK reception, and $\hat{\beta}_i$ represents the average number of trials and is derived as:

$$\hat{\beta}_i = \sum_{j=1}^{B_i} j [1 - [1 - P_s(i)]^{n_i}] [1 - P_s(i)]^{n_i [j-1]}, \quad (16)$$

where $P_s(i)$ have been derived in theorem 3.4.

IV. OPTIMIZED OPERATION CONTROL

From the battery lifetime analysis in (15), one sees that battery lifetime of devices may decrease in n_i and P_i because of the potential increase in the energy consumption per reporting period. Furthermore, when reliability of communication is lower than a threshold, increase in n_i and P_i may decrease the need for listening to the channel for ACK arrival and retransmissions, and hence, increasing n_i and P_i may increase the battery lifetime. Taking this into account, one sees there should be an operation point beyond which, increase in P_i and/or n_i offers a tradeoff between reliability and lifetime, and before it, increase in P_i and/or n_i increases both reliability and durability of communications. This observation will be evaluated using simulation results in the next section. Here, we aim at finding the optimized operation point of the network with respect to the battery lifetime. Using the battery lifetime definition in (15), one may define the optimization problem for deriving the optimized operating point of type i IoT devices as follows:

$$\begin{aligned} & \underset{n_i, P_i}{\text{maximize}} \quad \mathbb{L}(i); \\ & \text{s.t.: } P_o(i) \leq P_o^{\text{req}}(i), n_i \leq n_{\max}, P_i \leq P_{\max}, \end{aligned} \quad (17)$$

where $P_o^{\text{req}}(i)$ is the maximum tolerated outage probability for type i IoT devices. The reliability constraint in (17) could be rewritten as the minimum required success probability in communications as follows:

$$1 - n_i^{B_i} \sqrt{P_o^{\text{req}}}(i) \leq P_s(i). \quad (18)$$

Furthermore, by using the $P_s(i)$ expression in theorem 3.4, we have:

$$\begin{aligned} P_s(i) &= \int_0^\infty X_0 \exp(-X_5 r^2) 2r dr \\ &= \frac{0.5 \sqrt{\pi} \lambda_a \pi \exp(-\hat{v}_{i,2})}{\sum_k \lambda_k \hat{v}_{k,2} \left(\frac{P_k \gamma_{\text{th}}}{P_i \Omega} \right)^{0.5} \frac{\pi^2}{2} \csc\left(\frac{\pi}{2}\right) + \lambda_a \pi + \frac{N \gamma_{\text{th}}}{\Omega P_i \alpha}}, \end{aligned} \quad (19)$$

in which, $\ell_{\max} = 1$, $\delta = 2$, and $Q \approx 1$ have been assumed for brevity of expressions. Also, X_5 is an auxiliary variable equal to the denominator of (19). The expression in (19) could be rewritten as:

$$P_s(i) = \frac{D_0}{\frac{1}{\sqrt{P_i}} D_1 + \lambda_a \pi + \frac{N \gamma_{\text{th}}}{P_i \Omega \alpha}}, \quad (20)$$

where the auxiliary variables D_0 and D_1 are defined as:

$$\begin{aligned} D_0 &= 0.5 \sqrt{\pi} \lambda_a \pi \exp(-\hat{v}_{i,2}), \\ D_1 &= \sum_k \lambda_k \hat{v}_{k,2} \left(\frac{P_k \gamma_{\text{th}}}{\Omega} \right)^{0.5} \frac{\pi^2}{2} \csc\left(\frac{\pi}{2}\right). \end{aligned}$$

Satisfying (18) with equality, we have:

$$n_i^{B_i} \sqrt{P_o^{\text{req}}}(i) = 1 - \frac{D_0}{\frac{1}{\sqrt{P_i}} D_1 + \lambda_a \pi + \frac{N \gamma_{\text{th}}}{P_i \Omega \alpha}}.$$

TABLE I: Simulation Parameters

Parameters	Value
Service area	$20 \times 20 \text{ Km}^2$
Pathloss	$133 + 38.3 \log\left(\frac{x}{1000}\right)$
Thermal noise power	-174 dBm/Hz
Distribution of devices	PCP($\lambda_i \times 1e-6, 200$, Eq. (1) with $\sigma=100$)
Packet arrival of each device	Poisson distributed with average reporting period (T_i) of 300 s
Packet transmission time (τ_i)	100 ms
Signal BW	10 KHz
$E_0, P_c, E_{\text{st}} = 0.5 E_c$	1000 J, 10 mW, 0.1 J
P_r, P_a	0.5 W, 1.5 W
$\gamma_{\text{th}}, \varpi , \eta$	1, 1, 0.5
P_i, n_i, λ_a, W	Default: 21 dBm, 1, 5.5e-8, 100 KHz
ℓ_{\max}, Q	1, 0

By simplifying the expression, n_i is derived as a function of B_i as follows:

$$n_i = \left\lceil \log\left(\sqrt{B_i} \sqrt{P_o^{\text{req}}}\right) / \log\left(1 - \frac{D_0}{\frac{1}{\sqrt{P_i}} D_1 + \lambda_a \pi + \frac{N \gamma_{\text{th}}}{P_i \Omega \alpha}}\right) \right\rceil. \quad (21)$$

Also, the constraint on n_i is translated to a constraint on P_i as:

$$P_i \geq P_{\min} \triangleq \left(\frac{-D_1 + \sqrt{D_1^2 - 4 \frac{N \gamma_{\text{th}}}{\Omega \pi} \left(\lambda_a \pi - \frac{D_0}{1 - n_{\max}^{B_i} \sqrt{P_o^{\text{req}}}} \right)}}{2 \left(\lambda_a \pi - \frac{D_0}{1 - n_{\max}^{B_i} \sqrt{P_o^{\text{req}}}} \right)} \right)^2.$$

Then, the optimization problem in (17) reduces to a simple search over $P_{\min} \leq P_i \leq P_{\max}$ for minimization of :

$$\hat{\beta}_i E_c + \hat{\beta}_i n_i (\eta P_i + P_c) \tau_i, \quad (22)$$

in which n_i has been found as a function of P_i in (21), $\hat{\beta}_i$ has been found as a function of $P_s(i)$ and n_i in (16), and $P_s(i)$ has been found as a function of P_i in (20). This operation control optimization problem is investigated numerically in the next section (Fig. 2).

V. PERFORMANCE EVALUATION

In order to investigate usefulness of our findings in IoT-network planning and operation control, here we implement a MATLAB simulator for a heterogeneous IoT network. In our simulator, 2 types of IoT devices have been considered, that differ in the distribution processes describing locations of their respective nodes, and communications' parameters such as transmit power. Motivations for this setup are the coexistence of IoT technologies over the public ISM spectrum, e.g. SigFox and LoRa [7], and the coexistence of different IoT services over cellular networks, which are sharing a set of uplink resources, as described in [6]. For type i , the distribution process of locations is characterized by PCP($\lambda_i, v_i, f(x)$), where λ_i is the density of cluster points (in Km^{-2}), $v_i = 200$ is the average number of nodes in each cluster, and distribution of cluster nodes around the cluster center, i.e. $f(x)$, is modeled by a normal distribution with standard deviation of 100 meters. The reliability constraint is described as $p_s(i, d_{\text{eg}})$, where

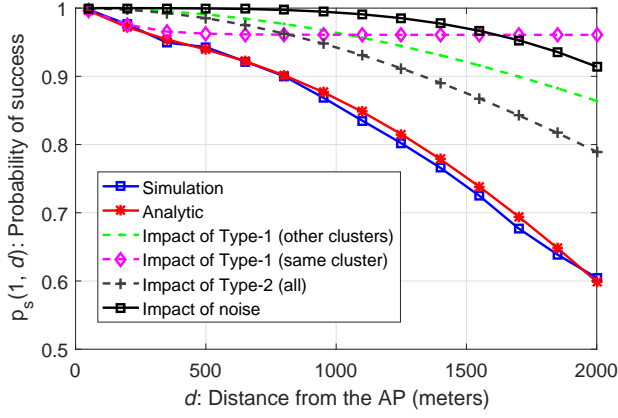
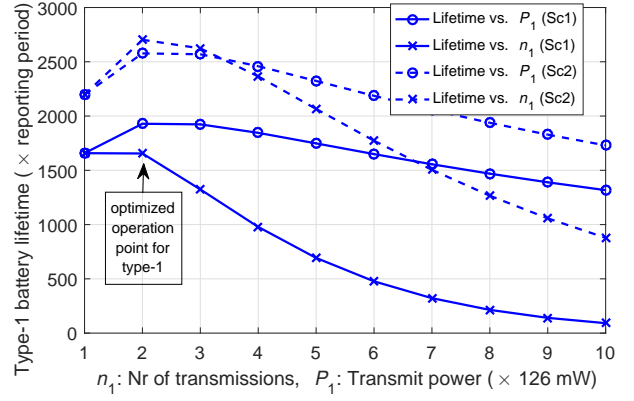


Fig. 1: Validation of analytical and simulation results. Device distribution: $K=2$, $\lambda_1=0.19$, $\lambda_2=3.8$, $v_1=1200$, $v_2=30$, $P_1=21$ dBm, and $P_2=25$ dBm.

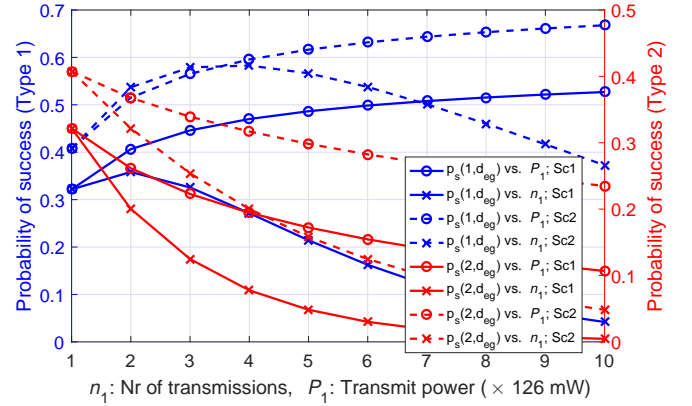
$d_{eg} = \sqrt{1/(\pi\lambda_a)}$ is equivalent to the cell-edge communication distance in the case of grid deployment of APs. The packet arrival at each node follows a PPP with rate $\frac{1}{T_i}$. The default values of other parameters can be found in Table I.

First, we investigate tightness of the derived analytical expressions. By considering an IoT network comprising of two IoT types with different distributions and transmit powers, Fig. 1 represents probability of success in packet transmission for type-1 as a function of distance from the AP. One sees that the analytical model matches well with the simulation results. We have further depicted the contributions of noise, interferences from the same and other clusters of type-1 devices, as well as interference from type-2 devices. Regarding the fact that transmit power of type-2 devices is 4 dB higher than type-1 devices in this figure, it is clear that interference from type-2 traffic (plus-marked curve) is the most limiting factor.

Fig. 2 represents the interplay among success probability, battery lifetime, n_i , and P_i . The x -axis in Fig. 2a and Fig. 2b represents P_1 for circle-marked curves, and n_1 for cross-marked curves. In these figures, Sc1 and Sc2 differ in density of type-2 devices, which is 2.4 in Sc1, and 1.2 in Sc2. One observes in Fig. 2a that battery lifetime is a quasi-concave function of both P_i and n_i . Furthermore, in Sc1, where density of nodes is higher than Sc2, battery lifetime decreases significantly by increase in the number of replica transmissions. In both scenarios, we see that the energy-optimized operation strategy for type-1 devices is to send 2 replicas per data packet to maximize their battery lifetimes. Fig. 2b represents the success probability for type-1 and type-2 traffic as a function of n_1 and P_1 . One sees that success probability for type-1 increases to a point beyond which, the resulting interference from extra transmitted packets starts deteriorating the performance. On the other hand, increase in the transmit power for type-1 devices, increases the success probability for this type and severely decreases the performance of type-2 devices. It is also worthy to note that in Fig. 2b, success probability increases in n_1 till $n_1 = 4$, however, from the



(a) Battery lifetime for type-1



(b) Probability of success in transmission for type-1 and type-2 devices

Fig. 2: Optimized operation control ($K = 2$, $\lambda_2=2.4$, $\lambda_1=2.4$ in Sc1 and $\lambda_1=1.2$ in Sc2). In circle-marked curves, $n_1 = 1$ and P_1 is varying. In plus-marked curves, $P_1 = 126$ mW and n_1 is varying.

battery lifetime analysis in Fig. 2a, it is evident that battery lifetime decreases in n_1 for $n_1 \geq 3$. To conclude, we see that increase in the number of replica transmissions, i.e. n_1 , increases both battery lifetime and reliability for $n_1 \in \{1, 2\}$, offers a tradeoff between battery lifetime and reliability for $n_1 \in \{3, 4\}$, and decreases both reliability and battery lifetime for $n \geq 5$. These results confirm importance of the derived results in this work, as they shed light to the operation point after which, it is not feasible to trade battery lifetime in hope of reliability.

Scalability analysis has been presented in Fig. 3. The analytical model of reliability has been found in (14) as a function of: i) transmit power, ii) number of replica transmissions, iii) density of APs, and iv) bandwidth of communications. Fig. 3 represents the rate at which, the amount of provisioned resources at the network-side, or energy resources at the device-side, could be scaled to comply with the increase in the level of required reliability. It is clear that transmit power of devices could be increased up to a certain level in order to combat noise. However, beyond a certain point, increase

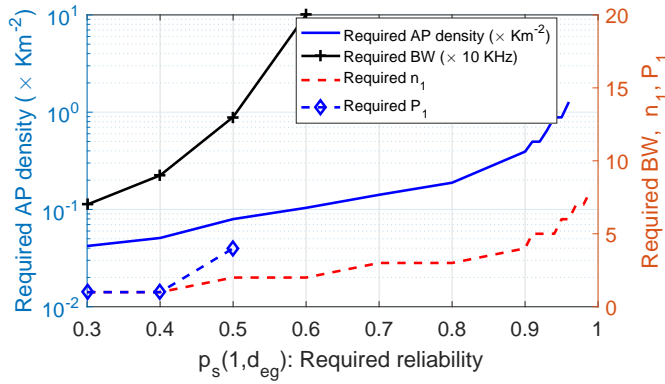


Fig. 3: Scalability analysis versus required reliability ($K = 1$, $\lambda_1 = 3.2$).

in the transmit power cannot increase the success probability because it cannot compensate the impact of interference. On the other hand, one sees that increase in the number of replicas per packet could be leveraged to increase reliability of communications. However, there is a saturation point in scenarios with higher densities of nodes, where increasing number of replicas increases traffic load significantly, and may even reduce reliability of communications. Example of such event was observed in Fig. 2b for $n_1 \geq 5$. Finally, the rate of increase in reliability of communications by increasing the number of APs, which reduces the communications' distance, and increasing the bandwidth, which decreases the collision probability, could be observed in Fig. 3.

VI. CONCLUSION

A tractable analytical model of reliability in large-scale heterogeneous IoT networks has been presented as a function of IoT traffic intensity and access network's resources. This model has been employed to analyze the impacts of resource provisioning at the network-side and operation control at the device-side on reliability and battery lifetime of IoT devices. The derived expressions illustrate the rate of increase in reliability and battery lifetime achieved by increasing the bandwidth of communications and number of APs. Our analyses indicated that depending on the operating point, increasing transmit power and number of replica transmissions may increase both reliability and battery lifetime, offer a tradeoff between them, or decrease both of them. Then, we developed a lifetime-optimal operation control policy for IoT devices. The simulation results confirmed existence of such an optimal operation point before which, battery lifetime and reliability are increasing in transmit power and number of replica transmissions; while beyond that point, there is a tradeoff between them. Finally, we have presented the scalability analysis to figure out the bounds up to which, increasing the provisioned resources at the network-side, or increasing energy consumption of IoT devices per packet transfer, can compensate the impact of increase in number of devices or their required QoS. The tightness and tractability of

the derived expressions promote use of them in IoT-network planning and operation control.

REFERENCES

- [1] C. Mavroumoustakis, G. Mastorakis, and J. M. Batalla, *Internet of Things (IoT) in 5G mobile technologies*. Springer, 2016, vol. 8.
- [2] W. Yang *et al.*, "Narrowband wireless access for low-power massive internet of things: A bandwidth perspective," *IEEE Wireless Commun.*, vol. 24, no. 3, pp. 138–145, 2017.
- [3] A. Laya, L. Alonso, and J. Alonso-Zarate, "Is the Random Access Channel of LTE and LTE-A Suitable for M2M Communications? A Survey of Alternatives," *IEEE Communications Surveys Tutorials*, vol. 16, no. 1, pp. 4–16, Jan. 2014.
- [4] A. Azari *et al.*, "Network lifetime maximization for cellular-based M2M networks," *IEEE Access*, vol. 5, pp. 18 927–18 940, Sept. 2017.
- [5] 3GPP TR 45.820, "Technical Specification Group GSM/EDGE Radio Access Network; Cellular system support for ultra-low complexity and low throughput Internet of Things (CIoT)," 2015.
- [6] 3GPP TSG RAN WG1, "Overall solutions for UL grant free transmission," Tech. Rep., June 2017.
- [7] M. Lauridsen, B. Vejlgaard, I. Z. Kovacs, H. Nguyen, and P. Mogensen, "Interference measurements in the european 868 MHz ISM band with focus on LoRa and SigFox," in *IEEE WCNC*, 2017, pp. 1–6.
- [8] M. Masoudi *et al.*, "Grant-free Radio Access IoT Networks: Scalability Analysis in Coexistence Scenarios," in *IEEE Global Communications Conference*, 2018, pp. 1–5.
- [9] H. Tabassum *et al.*, "Non-orthogonal multiple access (NOMA) in cellular uplink and downlink: Challenges and enabling techniques," *arXiv preprint arXiv:1608.05783*, 2016.
- [10] Z. Ding *et al.*, "A survey on non-orthogonal multiple access for 5G networks," *IEEE Journal on Selected Areas in Communications*, vol. 35, no. 10, pp. 2181–2195, 2017.
- [11] R. Karaki, A. Mukherjee, and J. F. Cheng, "Performance of autonomous uplink transmissions in unlicensed spectrum LTE," in *IEEE Global Communications Conference*, Dec 2017, pp. 1–6.
- [12] P. Popovski, *et al.*, "Ultra-Reliable Low-Latency Communication (URLLC): Principles and Building Blocks," *arXiv preprint arXiv:1708.07862*, 2017.
- [13] A. Azari, P. Popovski, G. Miao, and C. Stefanovic, "Grant-Free Radio Access for Short-Packet Communications over 5G Networks," in *IEEE Global Communications Conference*. IEEE, 2017, pp. 1–5.
- [14] G. Miao *et al.*, "E2MAC: Energy Efficient Medium Access for Massive M2M Communications," *IEEE Trans. on commun.*, vol. 64, no. 11, pp. 4720–4735, 2016.
- [15] Z. Li *et al.*, "2D time-frequency interference modelling using stochastic geometry for performance evaluation in low-power wide-area networks," *arXiv preprint arXiv:1606.04791*, 2016.
- [16] Y. Zhang, K. Peng, Z. Chen, and J. Song, "SIC vs. JD: Uplink NOMA techniques for M2M random access," in *IEEE ICC*, May 2017, pp. 1–6.
- [17] V. Suryaprakash *et al.*, "On the modeling and analysis of heterogeneous radio access networks using a poisson cluster process," *IEEE Trans. on Wireless Commun.*, vol. 14, no. 2, pp. 1035–1047, 2015.
- [18] C. Saha, M. Afshang, and H. S. Dhillon, "Poisson cluster process: Bridging the gap between PPP and 3GPP HetNet models," in *Information Theory and Applications Workshop (ITA)*, 2017. IEEE, 2017, pp. 1–9.
- [19] R. K. Ganti and M. Haenggi, "Interference and outage in clustered wireless ad hoc networks," *IEEE Trans. on Inf. Theory*, vol. 55, no. 9, pp. 4067–4086, 2009.
- [20] F. Baccelli, B. Błaszczyszyn, and P. Muhlethaler, "An aloha protocol for multihop mobile wireless networks," *IEEE Trans. on Inf. Theory*, vol. 52, no. 2, pp. 421–436, 2006.
- [21] A. Azari, M. Masoudi, and C. Cavdar, "Optimized Resource Provisioning and Operation Control for Low-power Wide-area IoT Networks," 2018, arXiv preprint arXiv:1804.09464.
- [22] I. S. Gradshteyn and I. M. Ryzhik, *Table of integrals, series, and products*. Academic press, 2014.
- [23] M. Haenggi, "On distances in uniformly random networks," *IEEE Trans. Inf. Theory*, vol. 51, no. 10, pp. 3584–3586, 2005.
- [24] 3GPP, "USF capacity evaluation for MTC," Tech. Rep., 2010, TSG GERAN 46 GP-100894.